Polysaccharide assisted microencapsulation for volatile phase change materials with a fluorescent retention indicator

Zhang, Yan; Jiang, Zhu; Zhang, Zhibing; Ding, Yulong; Yu, Qinghua; Li, Yongliang

[Link to publication on Research at Birmingham portal](#)

Accepted Manuscript

Polysaccharide Assisted Microencapsulation for Volatile Phase Change Materials with a Fluorescent Retention Indicator

Yan Zhang, Zhu Jiang, Zhibing Zhang, Yulong Ding, Qinghua Yu, Yongliang Li

Please cite this article as: Y. Zhang, Z. Jiang, Z. Zhang, Y. Ding, Q. Yu, Y. Li, Polysaccharide Assisted Microencapsulation for Volatile Phase Change Materials with a Fluorescent Retention Indicator, *Chemical Engineering Journal* (2018), doi: https://doi.org/10.1016/j.cej.2018.11.054

Polysaccharide Assisted Microencapsulation for Volatile Phase Change Materials with a Fluorescent Retention Indicator

Yan Zhang, Zhu Jiang, Zhibing Zhang*, Yulong Ding, Qinghua Yu and Yongliang Li*

School of Chemical Engineering, University of Birmingham, Edgbaston, Birmingham, West Midlands, U.K., B15 2TT

*corresponding author: Z.Zhang@bham.ac.uk, Y.Li.1@bham.ac.uk

ABSTRACT Low freeze point paraffin-based phase change materials (PCMs) for thermal energy storage often have very high vapor pressure, rendering it extremely challenging to encapsulate. This work reports our success in fabricating amino resin microcapsules with low freeze point PCMs cargos. Our findings challenge the emulsifier selection criteria proposed a decade ago, and enable better understanding of the role of emulsifiers in the one-step encapsulation process without precondensate synthesis. A facile, low cost, efficient and efficacious screening method utilizing a fluorophore is reported here for fast examination of core retention without resorting to more complex but unnecessary quantification techniques. This

method is transferable to other encapsulation methods or materials as a qualitative analysis tool. We report two new emulsifiers, i.e. xanthan gum and methylcellulose, which contribute to successful encapsulation of volatile cargos via the one-step in situ polymerization route. The concentration of xanthan gum affects not only the capsule size, but also shell thickness and surface roughness. Most importantly, we have demonstrated with methylcellulose that carboxyl or anhydride moieties in emulsifiers are not essential for the one-step process, contrary to the literature. Capsules produced with methylcellulose also demonstrate superior thermal cycling fatigue resistance.

1. Introduction

In situ polymerization of amino resins has been widely used to encapsulate a large collection of oil phases for self-healing materials [1-4], energy storage [5-8] and electrophoretic displays [9-11]. There are principally two preparation routes: a two-step route comprising pre-condensate preparation in an alkaline solution followed by polymerization in an acidic environment [12]; a one-step route which abandons the precondensate synthesis but only initiates the polymerization from monomers under acidic catalysis [13]. Elimination of the precondensate synthesis offers the merits of time and cost reduction, making it a preferred route. However, selection of emulsifiers is crucial to ensure successful encapsulation since inappropriate candidates produce unsatisfactory or no capsules at all [14, 15]. This is especially important when highly volatile paraffin-based phase change materials (PCMs) with low freeze points are the target cargos.

Brown, *et al*. [1, 13] first reported using poly (ethylene-*alt*-maleic anhydride) to produce poly (urea formaldehyde) (PUF) capsules in one step. Yoshizawa, *et al*. [14] afterwards tested additional polymers including poly (acrylic acid), poly (methylvinylether-*alt*-maleic anhydride),

2

poly (methylvinylether-*alt*-maleic acid), poly (isobutylene-*alt*-maleic anhydride) and reported successful encapsulation with all of them. Even though there are no carboxyl groups among some of the aforementioned emulsifiers bearing anhydride moieties, hydrolysis of the maleic anhydride grafted on the polyolefin backbones, upon contact with water, can convert the functional group into its parent carboxylic acid [14]. It was therefore concluded that participation in chemical reactions from carboxyl moieties on emulsifier molecules is necessary [14], and the emulsifiers reported to date [3, 13-18] do seem to support this conclusion. Most researchers adopted either poly (ethylene maleic anhydride) reported by Brown *et al.* [1, 13] or other anionic carboxyl bearing polymers. However, it was neither demonstrated experimentally what chemical reactions were involved, nor elucidated why these reactions are exclusive to carboxyl moieties.

We hereby report two new emulsifiers and demonstrate that carboxyl moieties are not essential. It is hypothesized that the high viscosity in the aqueous phase near the oil surface the strong binding abilities imposed by such polysaccharides contribute to the low permeability. This contributes to better understanding of the mechanistic fundamentals in emulsifier selection, and lifted the previously imposed criteria and broadened the range of emulsifier candidates. We have also developed a facile but effective technique for fast tracking encapsulation, which is extremely useful and effective for routinely screening materials.

2. Materials and Methods

We used heptane as a model volatile small molecule PCM in this work because of the absence of carboxyl or hydroxyl groups. We selected xanthan gum (XG) and methylcellulose (MC) as emulsifiers. All materials and chemicals were used as received without further purification or treatment unless specified otherwise. The following materials and chemicals were purchased

from Sigma-Aldrich UK: Urea (U5128, ACS reagent grade 99.0-100.5%), formaldehyde solution (47608, for molecular biology, BioReagent, $\geq$ 36.0% in H_2O), poly(vinyl alcohol) (PVOH) (363170, M_w 13,000~23,000, 87~89% hydrolyzed), poly(acrylic acid) (PAA) (181285, average M_v ~ 450, 000), xanthan gum (G1253, from Xanthomonas campestris), heptane (246654, anhydrous, 99%), Nile red (72485, for microscopy), and methyl cellulose (M0262, viscosity 400 cP). Ammonium chloride was purchased from Scientific Laboratory Suppliers. Resorcinol (98%) was purchased from Acros Organics.

The following encapsulation protocol, adapted from literature [13, 15], was used for encapsulation:

The emulsifier solution was prepared by hydrating the required quantity of emulsifier for 150 g water based on concentration calculation, and dissolving the weighed emulsifier in 150 g distilled water (conductivity $\leq$ 2.00 µS/cm monitored by a Mettler Toledo SevenCompact conductivity meter) at room temperature via high shear homogenization (4000 rpm for 10 min with a Silverson L4RT homogenizer), followed by 10 min ultrasonication. 2.500 g urea, 0.250 g resorcinol and 0.250 g ammonium chloride (Sartorius Secura124-1S analytical balance) were dissolved in the emulsifier solution prepared. The solution was ultrasonicated for 10 min and kept under stirring (IKA® RCT digital magnetic stirrer). The solution pH was adjusted to 3.50 ±0.02 (Mettler Toledo FiveEasy pH meter) with HCl solutions of various concentrations, and NaOH usage was avoided whenever possible to minimize the variation of ionic strength. Meanwhile the oil phase was prepared by dissolving approximately 1 mg Nile red inside 10 mL heptane under ultrasonication for 10 min. The core solution was then injected into the prepared aqueous solution via a syringe with a needle at a flow rate of 0.2 mL/s while under homogenization at 1200 rpm for 20 min (Silverson L4RT homogenizer).

Subsequently the prepared emulsion was transferred into a 250 mL jacketed beaker. A Rushton turbine (IKA R3004 stirrer diameter Φ30 mm) blade was used to keep the emulsion under stirring at 600 rpm (IKA Eurostar Labortechnik). 6.5 mL formaldehyde solution was added into the jacketed beaker, which was then covered with Al foil. The jacketed beaker was connected with a Julabo ME-F25 water bath programed as follows: the temperature was maintained at 20 ℃ for 30 min, then ramped up to 55 ℃ (1 ℃/min), maintained at 55 ℃ for 4 h and then cooled down to 20 ℃ (-1 ℃/min). The dispersion was then centrifuged four times at 6000 rpm (relative centrifugal force (RCF) 4180) for 5 min and vacuum filtered with 5 L of water. The harvested capsules were re-dispersed back in an aqueous environment for storage and dried under ambient conditions upon request.

The emission spectra of Nile red were obtained on a Nikon Eclipse Ti fluorescence microscope with a 457.9 nm excitation laser. A CoolLED pE-300 SB LEDs illumination system with a Leica DMRBE microscope was used for fluorescence microscopy (FM). The excitation maxima $\lambda_{ex\ max}$ = 460 nm. A H3 filter cube for the violet/blue excitation range (excitation filter BP 420-490) with a dichromatic mirror (510) and suppression filter (LP 515) was used as the FM setup configuration. This configuration allowed excitation wavelengths longer than 515 nm to pass. The morphology and shell surface of the microcapsules, along with shell thickness, were characterized with a Hitachi TM3030 tabletop SEM. Shell thickness at a higher resolution was characterized on a Philips ESEM electron microscope. The size distribution of microcapsules and poly (urea formaldehyde) (PUF) precipitates was monitored using Malvern Mastersizer 2000 with a wet dispersion unit.

Fourier transform infrared spectroscopy (FTIR) was performed on a Bruker Tensor 27 spectrometer to collect the vibration modes of functional groups within 400~4000 cm^{-1}. The

5

dynamic viscosity (shear viscosity) of the bulk aqueous phases was measured with a TA Instrument AR-G2 rheometer with a concentric cylinder measuring unit in the double gap configuration within a shear rate range $100\sim1000$ s^{-1} at 20˚C. Thermogravimetric analysis (TGA) was performed at 25 ºC on Linseis STA with an argon flushing gas at 10 ml/min. DSC thermogram was recorded on a Mettler Toledo DSC 3 instrument with liquid nitrogen as a coolant. Heating and cooling rates were set to 5 ºC/min.

3. Microcapsule Synthesis and Characterization

3.1 Fluorescent Spectroscopy and Microscopy

Quantification techniques such as UV spectroscopy or differential scanning calorimetry (DSC) are usually used for qualitative confirmation of successful encapsulation. We hereby report a simple method for this purpose when quantification is not required.

Nile red exhibits variation of its spectral position, shape and intensity according to the nature of dissolving solvents in attribution to the sensitivity of the polar substituents on its aromatic rings to its solvent environment [19-21]. When excited in its non-solvated form by a blue light ($\lambda_{ex\ max}$ = 460 nm), Nile red appears red under our current FM configuration. A green color reveals for excitation of its solvated form in heptane. This was confirmed by the fluorescence spectra and micrographs shown in Figure 1. Although the fluorescence spectra were obtained with excitation by a slightly different wavelength, it is generally believed to be insensitive to the excitation wavelength according to Kasha's rule [22, 23]. Tthe spectra of both non-solvated and solvated Nile red feature additional peaks in the blue and violet regions. Nevertheless, by applying an appropriate filter, we singled out the distinctive wavelength region where characteristic colors corresponding to the success or failure of encapsulation could be distinguished.
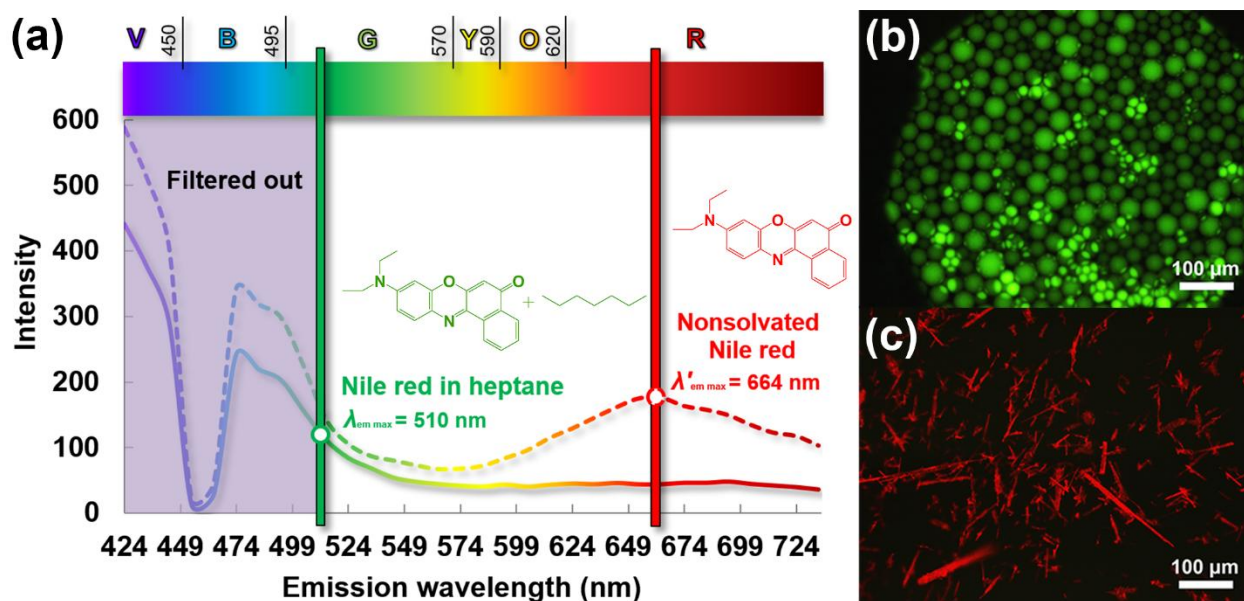
6

Figure 1 (a) Fluorescence spectra of non-solvated Nile red (dashed line) and solvated Nile red in heptane (solid line) within the emission wavelength range 424~735 nm; fluorescent microscopy (FM) images of (b) a heptane-in-water emulsion and (c) non-solvated Nile red.

3.2 Microencapsulation with Polysaccharides

Capsules were formed with 0.1 *wt*.% XG (Figure 2 (a$_1$) and (a$_2$))), but could not survive drying (Figure 2 (a$_3$) and (a$_4$)). Bright-field and fluorescent microscopy images complemented the results to be presented later that the collapsing observed in the SEM micrographs was probably not caused by the vacuum conditions. In order to improve capsule quality, XG concentration was varied between 0.1 *wt*.% and 0.01 *wt*.%. Lower concentrations produced capsules of superior strength to survive drying. In order to demonstrate a color contrast between loaded and hollow capsules, a cover glass was used to crush them open after 24 h of drying. As shown in Figure 3 (b) and (c), the color rapidly shifted from green to orange. The contrast could also be observed in Figure 3 (d) with intact green capsules in the top left corner and orange-red crushed ones.
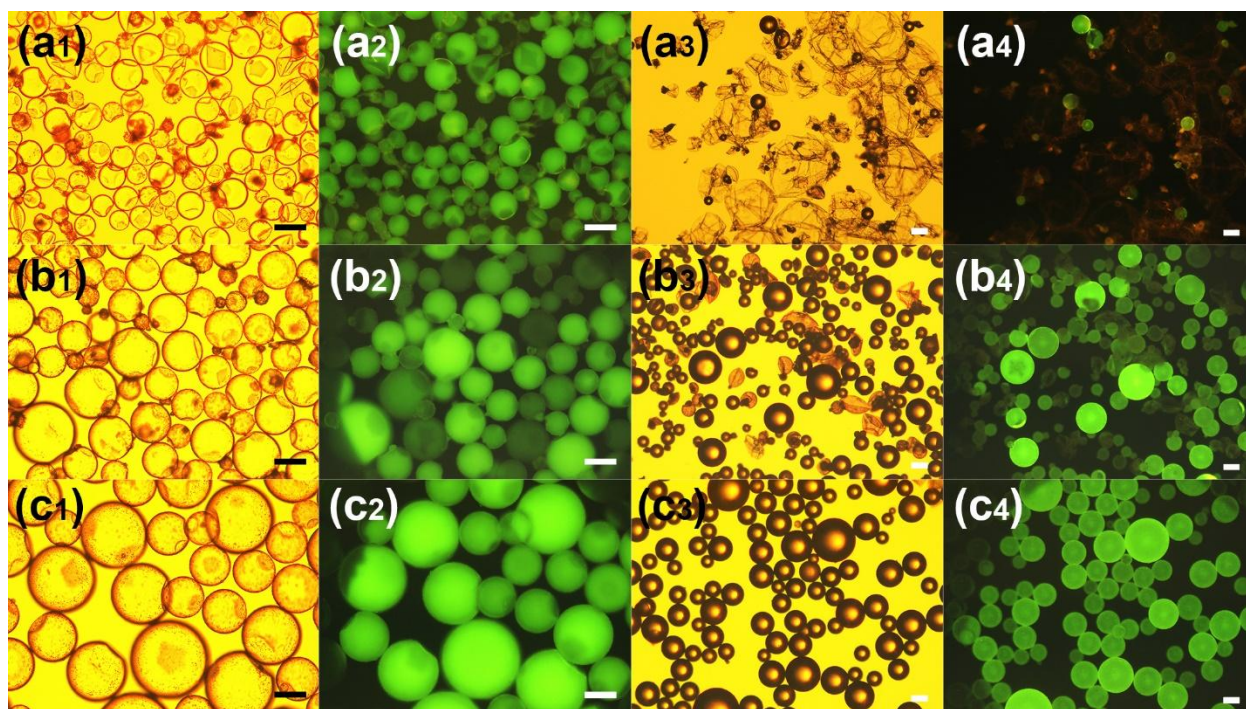
Figure 2 OM and FM micrographs of microcapsules formed with XG (a_1), (a_2) capsules dispersed in water (0.1 *wt*.% XG); (a_3), (a_4) capsules observed 24 h after drying (0.1 *wt*.% XG); (b_1), (b_2) capsules dispersed in water (0.05 *wt*.% XG); (b_3), (b_4) capsules observed 24 h after drying (0.05 *wt*.% XG); (c_1), (c_2) capsules dispersed in water (0.03 *wt*.% XG); (c_3), (c_4) capsules observed 24 h after drying (0.03 *wt*.% XG); (d_1), (d_2) capsules dispersed in water (0.01 *wt*.% XG); (d_3), (d_4) capsules observed 24 h after drying (0.01 *wt*.% XG). Images in the left two columns were captured at the same magnification (scale bars 50 µm); images in the right two columns were captured at the same magnification (scale bars 150 µm)
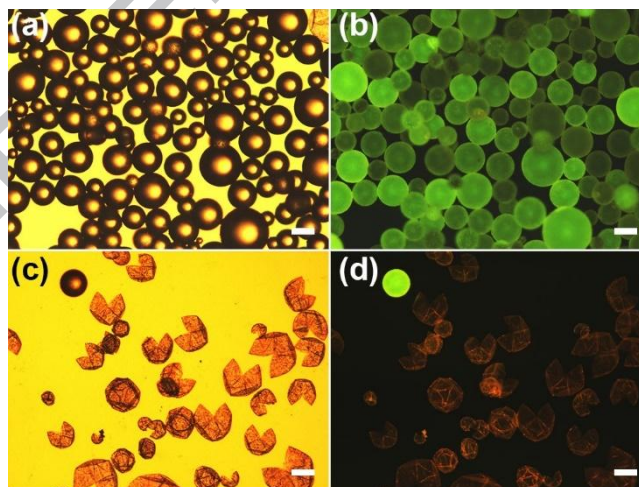

Figure 3 OM and FM micrographs of microcapsules formed with 0.01 *wt*.% XG (a), (b) capsules dried at ambient conditions for 24 h; (c), (d) capsules crushed open after 24 h.

Figure 4 (a_1) confirmed the insufficient strength of capsules produced with 0.1 *wt*.% XG. Most

particulate debris imbedded in the shell appeared to be up to several hundred nanometers with

some reaching 1~2 microns (Figure 4 (a_2)). Decreasing XG concentration to 0.05 *wt*.% and 0.01

wt.% reduced the quantity of collapsing capsules further, while enlarging the majority of

imbedding debris size into several microns, as well as the capsule size (Figure 4 (b_1)-(b_2) and

(c_1)-(c_2)). When the emulsifier concentration was high, the imbedding PUF particles could still

be seen from inside the capsules (Figure 4 (a_3) and (b_3)). They became much less prominent from

inside when the emulsifier concentration reduced (Figure 4 (c_3))..

Figure 4 SEM micrographs of heptane-PUF microcapsules along with their exterior and interior surface morphology formed with (a_1)-(a_3) 0.1 *wt*.% XG, (b_1)-(b_3) 0.05 *wt*.% XG, (c_1)-(c_3) 0.03 *wt*.% XG, and (d_1)-(d_3) 0.01 *wt*.% XG.

The critical concentration *C**, which is characteristic of the transition from dilute to semi-dilute

regimes featuring the first overlap and interaction of polymer molecules, has been reported to be

9

0.126 g/L (*ca.* 0.0126 *wt.*%) and 0.1 g/L (*ca.* 0.01 *wt.*%) for native and renatured XG respectively [24]. The critical concentrations C^{**} for the semi-dilute to concentrated regime transition are 0.78 g/L (*ca.* 0.078 *wt.*%) and 0.60 g/L (*ca.* 0.06 *wt.*%) for these two. [24] The XG concentrations used in our work spanned over all three regimes, with 0.01 *wt.*% in the dilute, 0.05 *wt.*% in the semi-dilute, and 0.1 *wt.*% in the concentrated regime. Even though capsules were found in all three regimes, it was obvious from Figure 4 that the capsules strength increased with decreasing concentration and optimal capsules tended to form at lower concentrations in the semi-dilute or dilute regimes. We identified 0.1 *wt.*% as the concentration at which capsule collapsing was too severe to be ignored for XG.

0.05 *wt.*% MC also proved successful as an emulsifier, confirmed by Figure 5 and Figure 6. After 24 h of ambient conditioned drying, capsule still assumed a green color (Figure 5 (f)) indicating the presence of heptane. Both exterior (Figure 6 (b)) and interior (Figure 6 (c)) surfaces appeared relatively smooth. The particles dotting around in the shell on the exterior surface were in the nanoscale and seemed to be more spherical than their counterparts when XG was used. Shell thickness also fell in the nanoscale, as shown in Figure 6 (c).

Capsule yield was calculated as the percentage of final dry capsule weight over the total weight of all materials used for synthesizing the shell including urea, formaldehyde, resorcinol, ammonium chloride, emulsifiers in addition to the heptane core. A yield of 16.3±4.2 % and 26.4±3.5% was achieved for 0.05 *wt.*% XG and 0.05 *wt.*% MC respectively.
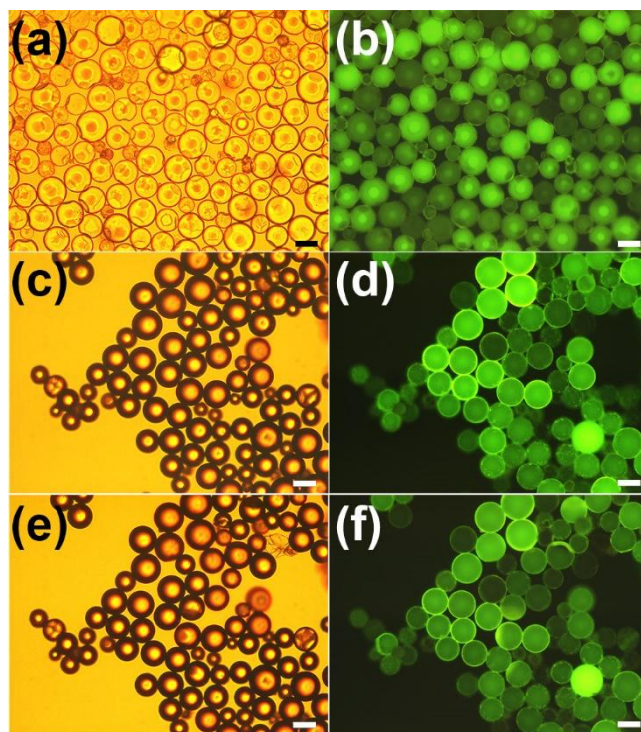
Figure 5 OM and FM micrographs of microcapsules formed with 0.05 *wt*.% MC (a), (b) capsules dispersed in water; (c), (d) capsules dried out of water immediately; (e), (f) capsules observed 24 h after drying. All images were captured at the same magnification (scale bars 50 μm).
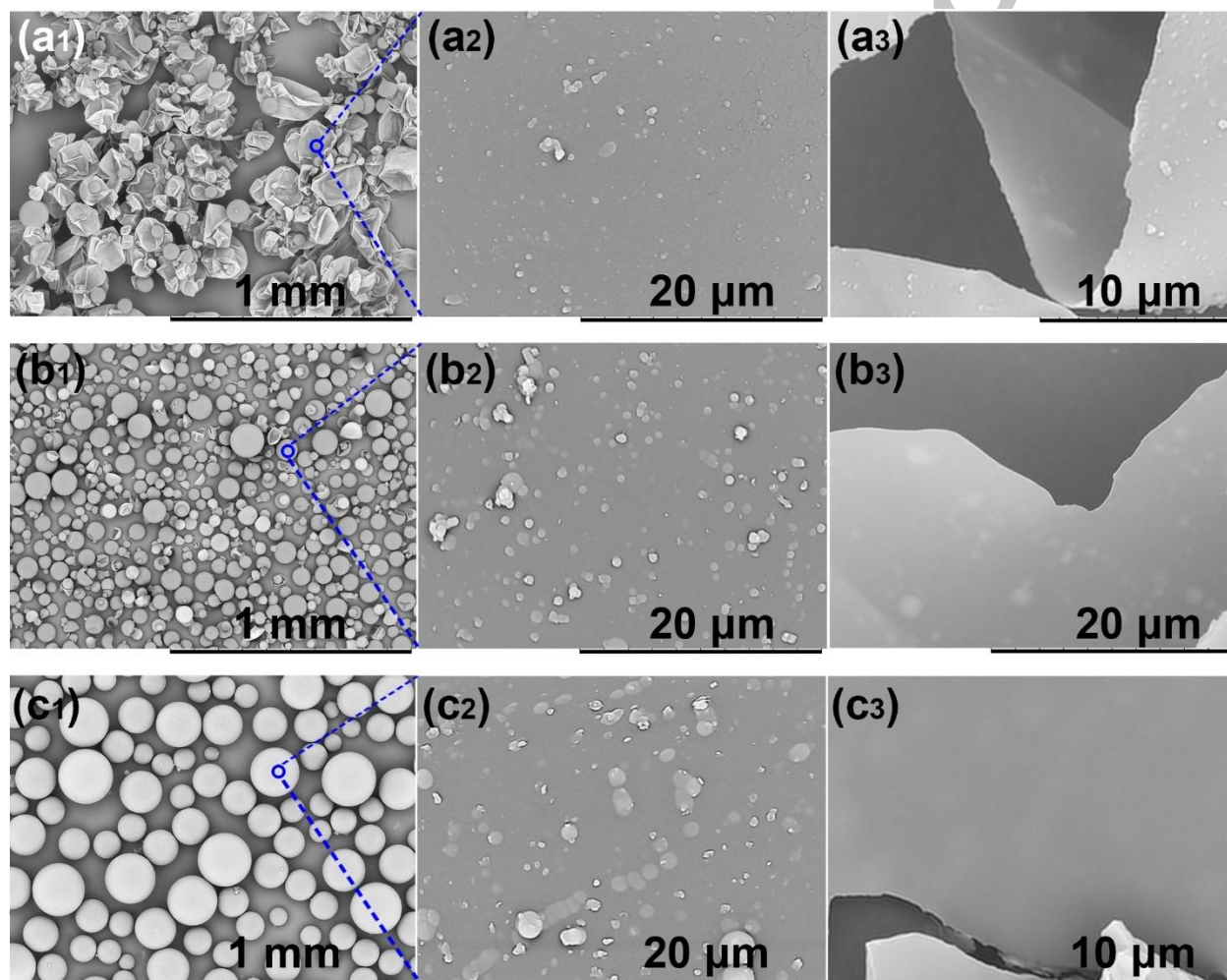

Figure 6 SEM micrographs of (a) heptane-PUF microcapsules along with their (b) exterior and (c) interior surface morphology formulated with 0.05 *wt*.% MC.

3.3 Fourier Transform Infrared Spectroscopy (FTIR)

MC is a polysaccharide consisting of linked glucose with hydroxyls and substituting methoxide [25], bearing no carboxyl moieties. In order to confirm the absence of other carboxyl bearing

11

contaminants, its ATR-IR spectrum in the range of 4000-400 cm^{-1} was presented in Figure 7.

PAA was used as a reference polymer bearing carboxyls.

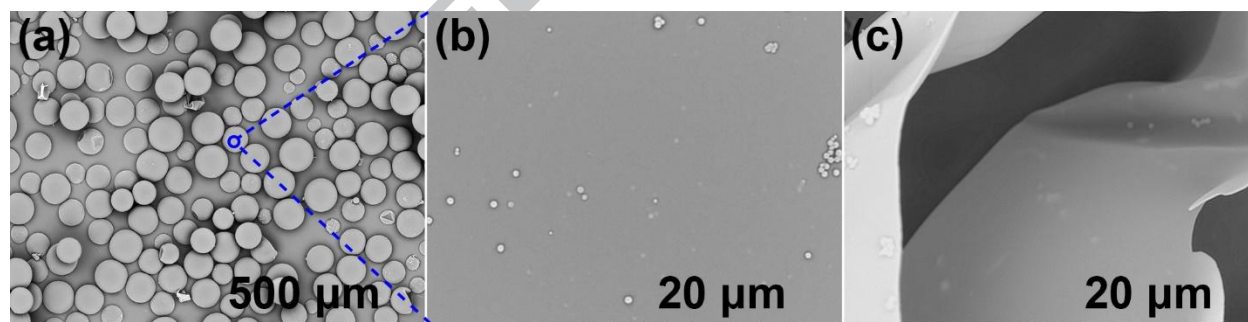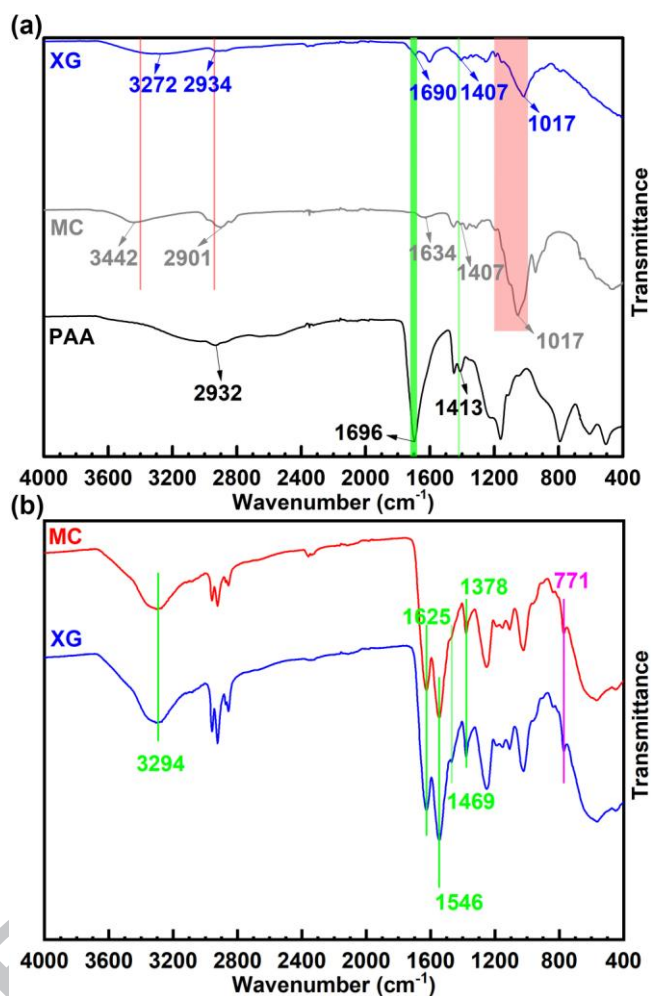Figure 7 FTIR-ATR spectra of (a) XG, MC and PAA (b) capsule shells formed with 0.05 *wt*.% XG and MC as the emulsifier. Green bands are characteristic of carbonyl moieties and pink bands are characteristic of polysaccharides.

FTIR bands around 3400 cm^{-1}, 2939 cm^{-1} and 990~1200 cm^{-1}, corresponding to the O-H and C-H stretching, prevails in all polysaccharides [26]. These bands could easily be identified in XG and MC. Carbonyls have a weak characteristic C-OH bending near 1420 cm^{-1} [27] and this could be observed at 1407 cm^{-1} for XG and 1413 cm^{-1} for PAA. Nevertheless, this range overlaps with the -CH$_2$ wagging and in-plane bending of -CH frequencies within 1411~1423 cm^{-1} [28] for carbohydrates. A very weak peak at 1407 cm^{-1} indeed was also identified in MC, which

12

prevented attribution of this band exclusively to the carbonyl moiety in carboxyl acids. The other distinctive peak associated with carbonyls derives from the asymmetric out-of-phase C=O stretching within 1680~1720 cm^{-1}, and is easily identified due to its strong intensity and insusceptibility to interference from other frequencies [27]. A strong IR band could be clearly identified at 1696 cm^{-1} for PAA A weaker peak for XG also appeared at 1690 cm^{-1}, arising from D-glucuronic acids within its molecules. This asymmetric out-of-phase C=O stretching band, however, was missing from MC, which provided evidence that carbonyls are absent insinuating no carboxyl moieties. The peak on the MC spectrum at 1634 cm^{-1}, close to the C=O out-of-phase stretching band, could either be the ring stretching of the monosaccharides in MC [26, 29], or scissoring from adsorbed water molecules [28, 30] as a result of its hygroscopic nature. Since this peak was very broad, similar to the -OH stretching vibration over 3000 cm^{-1}, we assigned this band to water molecules. Another implicit evidence that carboxylic acids are absent in MC could be inferred from the bandwidth and shift of the -OH stretching. The -OH stretching would shift to a lower wavenumber centering around 3000 cm^{-1} and become broader when a more strongly hydrogen-bonded –OH, such as in carboxylic acid, is present [27]. This was clearly manifested in the spectra of carboxyl-containing XG and PAA, where the –OH stretching in XG shifted to 3272 cm^{-1} and broadened, whereas both the shifting (to 2932 cm^{-1}) and broadening of this vibration were more prominent for PAA. A broad band was identified at 3442 cm^{-1} for MC, which was assigned to the claimed –OH stretching in hydrogen-bonded alcohols within 3230~3550 cm^{-1} [27]. There was no shifting to a lower wavenumber. The two characteristic bands for anhydrides involve the asymmetric out-of-phase and symmetric in-phase C=O stretching in the range 1750~1850 cm^{-1} [27]. MC showed no peaks within this region either.

The chemical structure of the shell was also characterized (Figure 7 (b)). The peaks between 2857 and 2958 cm^{-1} were in agreement with the FTIR spectrum of heptane [31] and accordingly assigned to the core PCM. This was likely caused by the residual heptane left during the FTIR sample preparation. The two broad peaks around 3294 cm^{-1} were difficult to be resolved individually but believed to be the –OH, –NH (weak) and –NH$_2$ (strong broad) stretching, which contained the characteristic amide bonds featuring the primary amide –NH$_2$ stretching around 3370~3200 cm^{-1} and a weak secondary amide –NH stretching peak around 3300 cm^{-1} [27]. Since the characteristic amide peaks from the crosslinking between urea and formaldehyde could not be easily resolved, the amide bond formation cannot be confirmed. Fortunately, additional characteristic IR bands for amides at 1625 cm^{-1} and 1546 cm^{-1}, were identified in urea formaldehyde [17, 32]. Primary amide bonds have bands near 1610 cm^{-1} and 1410 cm^{-1} corresponding to the NH$_2$ bending and C-N stretching respectively [27]. There were two peaks on the IR spectrum at 1625 cm^{-1} and 1378 cm^{-1} that likely corresponded to these two frequencies, which were similar to the peaks observed at 1650 cm^{-1} and 1380 cm^{-1} by Fan, *et al*. [32]. The weak peak at 1469 cm^{-1} was assigned to the bending of methylene bridge in the N-CH$_2$-N group [17]. The bands at 1546 cm^{-1} were postulated to be the C-NH bending and C-N stretching from the non-cyclic secondary amide group. The multiple peaks at 1109 cm^{-1}, 1154 cm^{-1}, 1188 cm^{-1} and 1251 cm^{-1} within the 1050~1300 cm^{-1} region very likely involved the in-plane movement of the benzene ring carbons and substituents. The 620~850 cm^{-1} region corresponded to the out-of-phase ring vibration and differentiated the ortho, meta and para isomers around 750 cm^{-1}, 775 cm^{-1} and 800 cm^{-1} respectively [27, 33]. The peak in the IR spectra of microcapsule shells at 771 cm^{-1} confirmed the meta isomer of the benzene ring, which originated from resorcinol. All these confirmed the participation of resorcinol in the polymerization reaction.

14

3.4 Dynamic Viscosity

The shear stress and dynamic viscosity of various emulsifier solutions are presented in Figure 8. 0.05 *wt*.% MC was treated to be Newtonian along with 0.1 *wt*.% PVOH and distilled water based on Figure 8 (a), while XG solutions of various concentrations clearly showed shear thinning behaviors. Figure 8 (b) confirmed that the dynamic viscosity decreased with shear rate at a fixed concentration and increased with XG concentration at a fixed shear rate. The dynamic viscosity of 0.05 *wt*.% MC was lower than XG solutions, but higher than 0.1 *wt*.% PVOH, which was nearly identical with distilled water. Within the shear rate range investigated, the majority of solutions had a viscosity lower than 0.01 Pa·s.
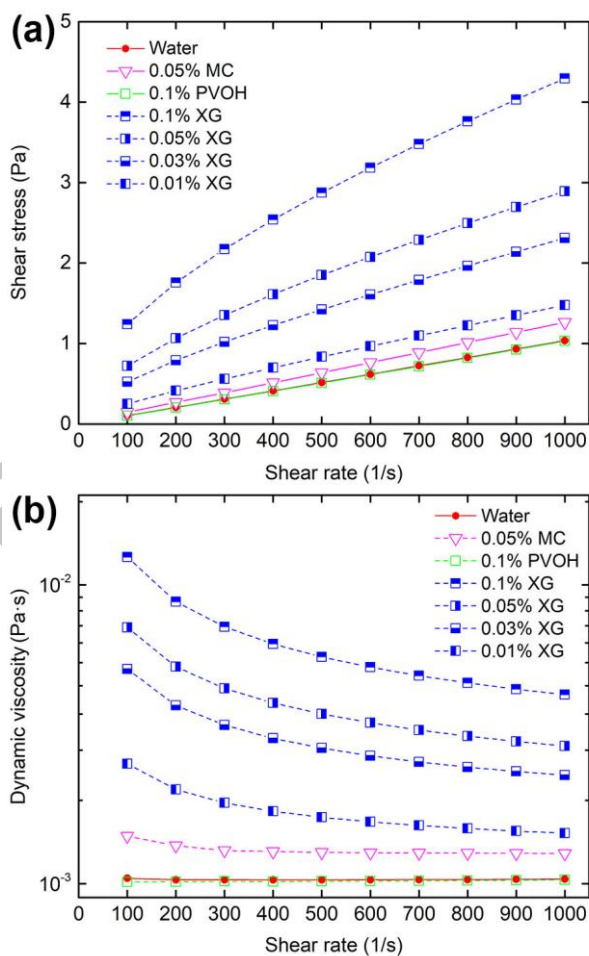

Figure 8 (a) Dynamic viscosity and (b) shear stress of XG solutions at various concentrations, 0.05 wt.% MC and 0.1 wt.% PVOH.

16

3.5 Laser Diffraction for Size Distribution

It is from Figure 9 that microcapsules typically had diameters in the order of tens of microns. Gum Arabic (GA) has also been reported successful previously in forming microcapsules[15]. But varying GA concentration from 0.05 *wt*.% to 0.2 *wt*.% showed no influence on size distribution [15]. Nevertheless, decreasing XG concentration in our work markedly enlarged capsules. Non-adsorbing polysaccharides such as XG [34] can stabilize the O/W interface by their viscosity modification of the aqueous phase [35, 36]. Nevertheless, MC is chemically modified with hydrophobic methyl groups, thus can stabilize an O/W interface via adsorption, in addition to its viscosity enhancement to the aqueous phase. Even though polysaccharides are not surfactants in a conventional sense, their concentrations still have a similar critical micelle concentration (CMC) effect. Interfacial tension decreases dramatically with the initial addition of adsorbing polysaccharides with surface activities and plateaus at a critical concentration [36]. The non-adsorbing behavior of XG renders it less effective to maintain a large surface to volume ratio owning solely to viscosity effect, especially at low concentrations, compared with GA. As the concentration reduced, the viscosity enhancing effect also diminished. This could be a reason for a marked effect of XG concentration on produced capsule size distribution in our work, as opposed to a negligible effect for GA.
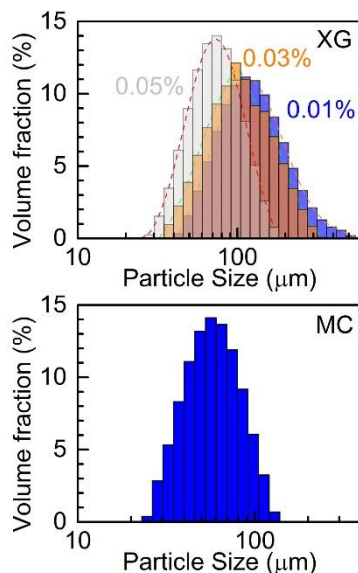
Figure 9 Size distribution of microcapsules formualted with 0.05 *wt*.%, 0.03 *wt*.% and 0.01 *wt*.% XG and 0.05 *wt*.% MC.

3.6 Dried Microcapsules

Most capsule-water slurries had silky textures, and were dried into flowing powders. Some agglomeration lumps could be observed in the MC slurry. This was likely caused by MC precipitation as a result of its lower critical solution temperature (LCST) within 40~50 ℃ [25], below our experimental condition 55 ℃. The flowing behavior was linked with the large capsule size, decently smooth surface and no noticeable solid bridges between them.

3.7 Shell Thickness

Thickness of the inner smooth region within capsule shells was insensitive to experimental parameters and was in the range of several hundred nanometers [13]. What we observed, however, was that XG concentration did affect this smooth region thickness, and it could increase into the microscale (Figure 10).
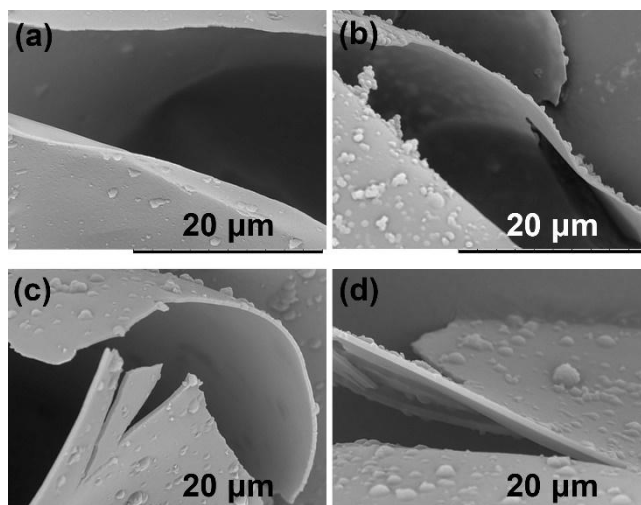
Figure 10 Shell thickness increase into the microscale (a) 0.1 *wt*.% XG, (b) 0.05 *wt*.% XG, (c) 0.03 *wt*.% XG and (d) 0.01 *wt*.% XG.

3.8 Core Leakage and Payload

Core leakage of microcapsules formed by 0.01 *wt*.% and 0.05 *wt*.% XG as well as 0.05 *wt*.% MC was studied by thermogravimetric analysis (TGA) as shown in Figure 11 (a). Capsules produced by 0.01 *wt*.% XG had the least leakage within 5 h of drying, with the sample formed by 0.05 *wt*.% XG being slightly more severe. The mass loss was both less than 8%. Microcapsules produced by 0.05 *wt*.% MC ranked at the top of leakage tests with a higher than 11% mass loss. A propensity of increasing leakage with decreasing shell thickness was generally observed attributing to a shorter diffusion path.

Based on the shell thickness (Figure 10 and Figure 11) and capsule size results (Figure 9), we estimated the theoretical payload, defined as the weight percentage of core in capsules, which was found to be at least 80%. Due to the high percentage and volatility of core heptane, the payload was quantified by the weight difference before and after mechanical compression of loose powders. The results were 90.1±1.2% and 92.2±1.1% respectively for 0.05 *wt*.% XG and MC.
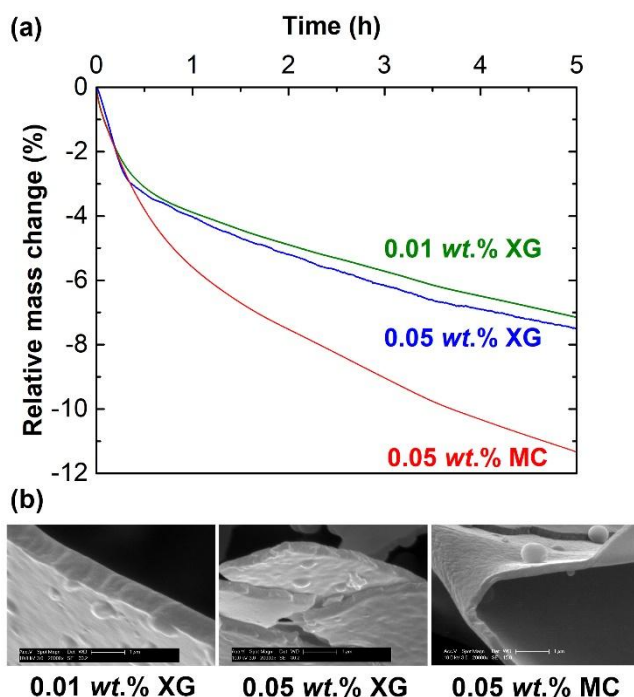
19

Figure 11 (a) Relative mass change of microcapsules formed with 0.01 wt.% XG, 0.05 wt.% XG and 0.05 wt.% MC as emulsifiers within 5 h at 25ºC recorded by TGA; (b) high resolution SEM micrographs of shell thickness of the aforementioned three batches of microcapsules. (scale bars 100 µm)

3.9 Mechanism Discussion

It was believed that carboxyl, but not hydroxyl moieties, can provide reaction sites for the polymerization of shell growth [14, 16]. We already knew the presence of D-glucuronic acid in XG. Aldobionic [37] and diferulic acid [38] have been identified in GA. These findings, along with other polymeric emulsifiers [3, 13-18] reported to date, do seemingly support the importance of carboxyl moieties [14]. However, the methylol urea products from the acid catalyzed urea-formaldehyde reaction [39] have been reported to be able to undergo further crosslinking with both hydroxyl and carboxyl groups [40]. Reactions between formaldehyde and PVOH [41], as well as amino resin and hydroxyl functionalized polyester [42] have also been reported. FTIR analysis confirmed benzene rings within capsule shells, only likely from

20

resorcinol. It is reasonable to believe that at least some hydroxyls can participate in the polymerization.

The surprising success achieved with MC bearing no carboxyls or anhydrides to synthesize microcapsules suggests that such moieties may not be essential.

We monitored the size distribution of PUF precipitates without heptane for miscellaneous emulsifiers, as demonstrated in Figure 12. Accurate interpretation of the results was difficult since the size evolution was not truly revealed, ascribing to agglomeration. The results were only used as a guidance to infer the precipitation growth and agglomeration tendency. The surface area moment mean (Sauter mean diameter) D[3,2] was preferred owing to its sensitivity to surface area. 0.01 *wt*.% XG did not effectively retard PUF agglomeration in the bulk continuous phase, as D[3,2] quickly increased in the initial stage (Figure 12) owing to the low viscosity (Figure 8 (a)). However, this did not prohibit XG from making positive contribution to the encapsulation. 0.1 *wt*.% PVOH showed fairly similar capability of viscosity modification of the bulk aqueous phase (Figure 8) and precipitation retardation (Figure 12). Nevertheless, the shell morphology was completely different (Figure 12 inset).
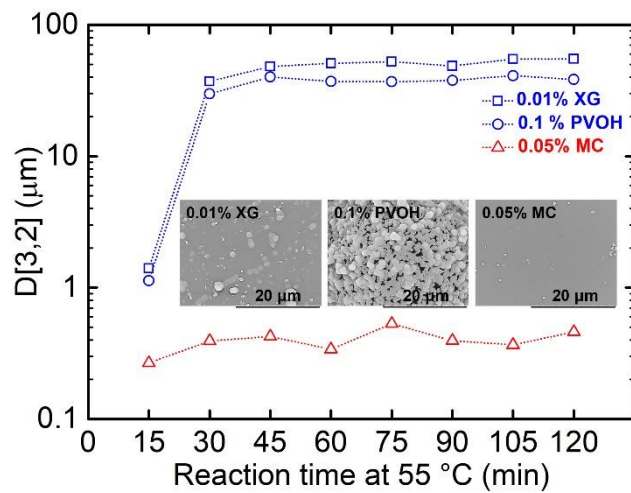
21

Figure 12 Size evolution of PUF precipitates in the bulk aqueous phase over reaction time at 55˚C.

We speculate that the interfacial rheology could be a key for compact shell formation. In addition, the similarity between the polysaccharides, XG and MC, lies in that they are normally used for thickening or gelling purposes, and both have strong water binding abilities [36, 43, 44]. The strong water and solute binding abilities could immobilize water molecules and monomers within its thin film network adsorbed at the O/W interface. Non-adsorbing polymers such as XG can also create a network around the colloidal droplets [45]. Viscosity of the oil rich regions was reported to be a thousand folds higher than the adjacent xanthan-rich regions at a concentration less than 0.1 *wt*.%[34, 46]. This suggests an increasing viscosity gradient from the bulk aqueous phase to the oil-rich phase, akin to the adsorbing polysaccharide MC.

If intercalated monomers in the polysaccharide network cross-link, the high viscosity in the oil adjacent aqueous phase slows down the chemical reaction, according to the simplified Smoluchowski equation [47], as a result of the reduced diffusion rate and probability or frequency of collision from monomer molecules in diffusion-controlled reactions:

$$k = 4\pi N R' D \tag{1}$$

where k is the rate constant of the bimolecular process in units $M^{-1}s^{-1}$, N is Avogadro's number per millimole, R' is the encounter distance roughly equivalent to the sum of the molecular radii, and D is the relative diffusion coefficient, which reduces to the Stokes-Einstein equation (2) for the scenario when the monomer molecules moving in a continuous medium are assumed to be particles of the size larger than their solvent counterparts [48]:

$$D = \frac{RT}{6\pi\eta r N_A} = \frac{k_B T}{6\pi\eta r} \tag{2}$$

where R is the gas constant, N_A is Avogadro's number, k_B is Boltzmann's constant, T is the absolute temperature in Kelvin, η is the dynamic viscosity and r is particle radius.

Introducing polysaccharides into the polycondensation reaction may also have brought in extra chemical reactions such as glycosylation between polysaccharides and hydroxyl groups. A more compact shell structure assisted by additional reactions would enable cross-linking from a molecular level and increasing the degree of cross-linking, rather than fusion of microscale particles. This could reduce permeation of the oil phase, even though the shell thickness was only hundreds of nanometers.

4. Thermal and Stability Characterization

4.1 Phase Transition

One sample prepared with 0.05 *wt.*% MC was dried at ambient conditions into a free flowing powder and stored in a sealed vial at 4 ℃ for 30 days before a leakage check. FM in Figure 13 (a) confirmed heptane retention by the large number of green microcapsules after 30 days. The phase transition was monitored with DSC from -80 to -140 ℃. Two separate peaks at -108.6 and -88.8 ℃ were identified for the exothermic cooling and endothermic heating processes respectively, with a supercooling of 19.8 ℃ (Figure 13 (b)). The normalized enthalpy of fusion was 150.6 and -147.4 J/g. The DSC thermogram provided further evidence for the successful encapsulation.
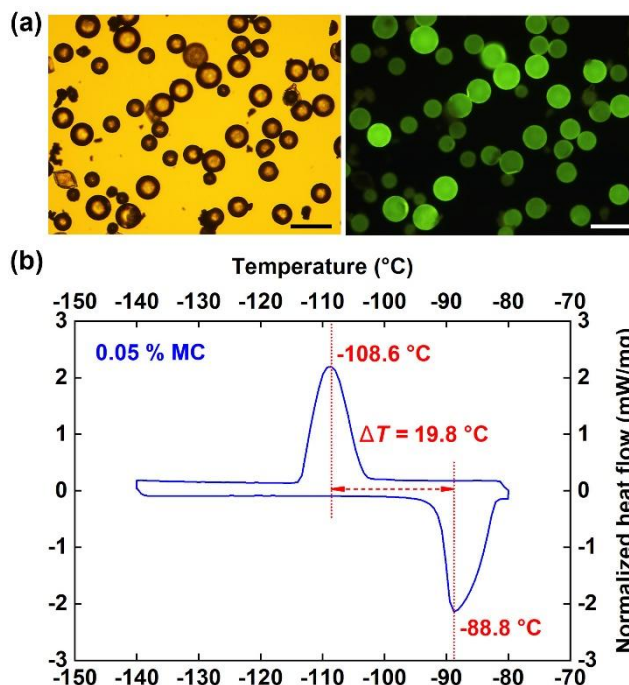
Figure 13 (a) OM and FM micrographs of PUF-heptane microcapsules formed with 0.05 wt.% MC after 30 days of storage in the dry powder form at 4 ºC (*scale bars 100 μm)*; (b) DSC thermogram (heating/cooling rate 5ºC/min) of PUF-heptane microcapsules after 30 days of storage in the dry powder form at 4 ºC.

4.2 Thermal and Mechanical Stability

Two samples were subject to 15 thermal cycles from 25 ºC to -140 ºC to ensure that phase

transition was inflicted repeatedly. Capsules produced with 0.05 *wt*.% XG did not show strong

fatigue resistance to survive the harsh cycling, confirmed by the red color emission in Figure 14

(b$_2$). Most capsules collapsed after cycling and released the volatile heptane, possibly through

cracks propagating from within the polymer shell. There were only a few green capsules still

containing heptane. With most microcapsules still assuming their original shape and a green

emission color, 0.05 *wt*.% MC, on the other hand, produced capsules of sufficient fatigue

resistance (Figure 14 (c$_2$ and(d$_2$)). Results suggest that there could be two potential reasons for

the better fatigue resistance demonstrated by the MC sample. One is that a thinner capsule shell

could impart more flexibility. Stress would concentrate at the deformation borderline on capsule

25

shells when they deflect in response to the pressure difference inflicted by a change of core

volume upon phase transition or leakage. The flexibility of thin shells permits it to bend without

initiation or propagation of cracking at least at an early stage. The other possibility of better

fatigue resistance could be that the type of emulsifiers selected may function as more effective

plasticizers of the shell.

DSC thermogram of 5 identical thermal cycles are presented in Figure 14 (e) and (f). The 0.05

wt.% XG sample featured a very small peak around -94 ~ -96 ºC during the first exothermic

cooling cycle. This peak intensity increased further with more thermal cycles. From cycle 2, a

separate peak around -103 ~ -104 ºC appeared as well. The multiple peaks are postulated to be

from leaking heptane. For the endothermic heating process, only one single phase transition

temperature was observed around -88 ºC. For the 0.05 *wt*.% MC sample, a small peak at -98.4 ºC

only started appearing from cycle 3 and increased mildly as cycling continued. The peak

intensity was quite low, insinuating slower leakage. The endothermic heating process again only

featured one single peak at -88.4 ºC. These results are in good agreement with fluorescent

microscopy images. It should be noted that the DSC results do not conflict with the evaporation

test obtained by TGA as shown in Figure 11. The leaking tests from TGA only revealed static

room temperature leaking, which indicated shell permeability only. However, dynamic induced

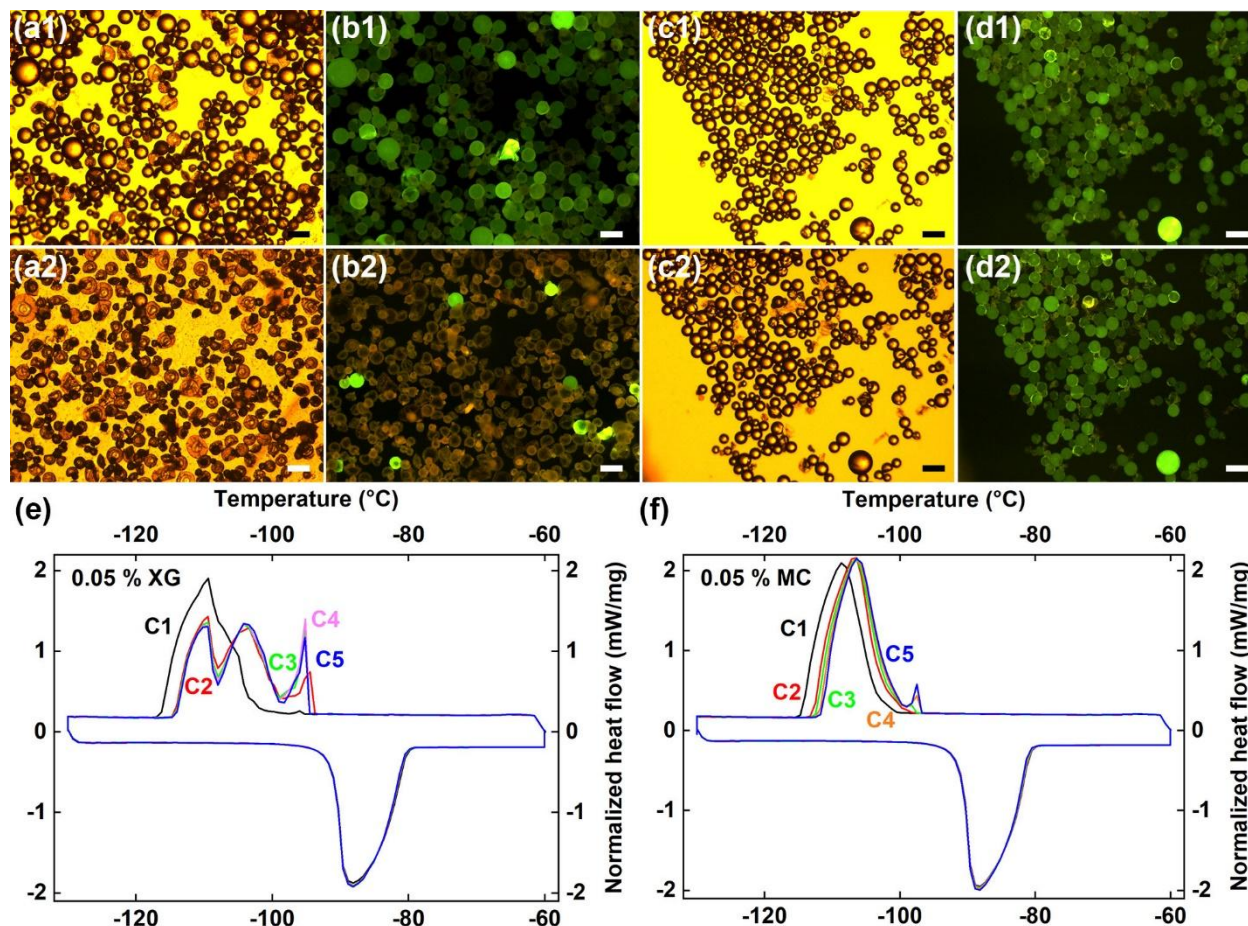additional leakage by fatigue cracking, which was more severe.

Figure 14 (a_1), (a_2) OM and (b_1), (b_2) FM images of microcapsules formed with 0.05 *wt*.% XG before and after cycling; (c_1), (c_2) OM and (d_1), (d_2) FM images of microcapsules formed with 0.05 *wt*.% MC before and after cycling (all scale bars 100 μm); (e), (f) DSC thermogram of microcapsules formed with 0.05 *wt*.% XG and MC for 5 cycles.

5. Conclusions

A fast and effective method of screening emulsifiers with Nile red for encapsulation of heptane via the one-step in-situ polymerization is reported here. The technique can be used with great ease to qualitatively determine if the encapsulation is successful after drying without resorting to more advanced techniques. It is especially beneficial for inspection of dried capsules when standard OM may lack the contrast if capsules have rough surfaces. We identified two new

27

emulsifiers, xanthan gum and methylcellulose, which are deemed suitable for the one-step in situ polymerization. We demonstrated that carboxyls and anhydrides in emulsifier molecules are not required, contrary to what has been reported in the literature. It is therefore proposed that the effect of polysaccharide emulsifiers on the formation of capsules and shell thickness is attributed to the viscosity imparted by such emulsifiers and their strong water and solute binding abilities. The monomers intercalated in the polymer network as a result of the polysaccharides' binding abilities facilitate slow cross-linking from a molecular level and retardation of rapid PUF precipitation in the interfacial region to form more compact and less porous shells. The thermal properties such as phase change temperatures and enthalpy of fusion were characterized with DSC and MC appears to offer better capsule performance under dynamic thermal cycling conditions compared with XG.

REFERENCES

[1] E.N. Brown, S.R. White, N.R. Sottos, Microcapsule induced toughening in a self-healing polymer composite, Journal of Materials Science 39 (2004) 1703-1710.

[2] C. Suryanarayana, K.C. Rao, D. Kumar, Preparation and characterization of microcapsules containing linseed oil and its use in self-healing coatings, Progress in Organic Coatings 63 (2008) 72-78.

[3] B.J. Blaiszik, M.M. Caruso, D.A. McIlroy, J.S. Moore, S.R. White, N.R. Sottos, Microcapsules filled with reactive solutions for self-healing materials, Polymer 50 (2009) 990-997.

[4] T. Nesterova, K. Dam-Johansen, S. Kiil, Synthesis of durable microcapsules for self-healing anticorrosive coatings: A comparison of selected methods, Progress in Organic Coatings 70 (2011) 342-352.

[5] G. Fang, H. Li, F. Yang, X. Liu, S. Wu, Preparation and characterization of nano-encapsulated n-tetradecane as phase change material for thermal energy storage, Chemical Engineering Journal 153 (2009) 217-221.

[6] F. Salaün, E. Devaux, S. Bourbigot, P. Rumeau, Influence of process parameters on microcapsules loaded with n-hexadecane prepared by in situ polymerization, Chemical Engineering Journal 155 (2009) 457-465.

[7] Y. Konuklu, H.O. Paksoy, M. Unal, S. Konuklu, Microencapsulation of a fatty acid with Poly(melamine–urea–formaldehyde), Energy Conversion and Management 80 (2014) 382-390.

[8] Z. Chen, J. Wang, F. Yu, Z. Zhang, X. Gao, Preparation and properties of graphene oxide-modified poly(melamine-formaldehyde) microcapsules containing phase change material n-dodecanol for thermal energy storage, Journal of Materials Chemistry A 3 (2015) 11624-11630.

[9] H.L. Guo, X.P. Zhao, Preparation of a kind of red encapsulated electrophoretic ink, Optical Materials 26 (2004) 297-300.

[10] H. Guo, X. Zhao, J. Wang, Synthesis of functional microcapsules containing suspensions responsive to electric fields, Journal of Colloid and Interface Science 284 (2005) 646-651.

[11] R. Qiao, X.L. Zhang, R. Qiu, Y.S. Kang, Synthesis of functional microcapsules by in situ polymerization for electrophoretic image display elements, Colloids and Surfaces A: Physicochemical and Engineering Aspects 313-314 (2008) 347-350.

[12] S.-J. Park, Y.-S. Shin, J.-R. Lee, Preparation and Characterization of Microcapsules Containing Lemon Oil, Journal of Colloid and Interface Science 241 (2001) 502-508.

[13] E.N. Brown, M.R. Kessler, N.R. Sottos, S.R. White, In situ poly(urea-formaldehyde) microencapsulation of dicyclopentadiene, Journal of Microencapsulation 20 (2003) 719-730.

[14] H. Yoshizawa, E. Kamio, E. Kobayashi, J. Jacobson, Y. Kitamura, Investigation of alternative compounds to poly(E-MA) as a polymeric surfactant for preparation of microcapsules by phase separation method, Journal of Microencapsulation 24 (2007) 349-357.

[15] C. Fan, X. Zhou, Effect of emulsifier on poly(urea–formaldehyde) microencapsulation of tetrachloroethylene, Polymer Bulletin 67 (2011) 15-27.

[16] H. Yoshizawa, E. Kamio, N. Hirabayashi, J. Jacobson, Y. Kitamura, Membrane formation mechanism of cross-linked polyurea microcapsules by phase separation method, Journal of Microencapsulation 21 (2004) 241-249.

[17] S. Cosco, V. Ambrogi, P. Musto, C. Carfagna, Properties of poly(urea-formaldheyde) microcapsules containing an epoxy resin, Journal of Applied Polymer Science 105 (2007) 1400-1411.

[18] S. Cosco, V. Ambrogi, P. Musto, C. Carfagna, Urea-Formaldehyde Microcapsules Containing an Epoxy Resin: Influence of Reaction Parameters on the Encapsulation Yield, Macromolecular Symposia 234 (2006) 184-192.

[19] M.M. Davis, H.B. Helzer, Titrimetric and Equilibrium Studies Using Indicators Related to Nile Blue A, Analytical Chemistry 38 (1966) 451-461.

[20] P. Greenspan, S.D. Fowler, Spectrofluorometric studies of the lipid probe, nile red, Journal of Lipid Research 26 (1985) 781-789.

[21] T.J. Zuehlsdorff, P.D. Haynes, M.C. Payne, N.D.M. Hine, Predicting solvatochromic shifts and colours of a solvated organic dye: The example of nile red, The Journal of Chemical Physics 146 (2017) 124504.

[22] M. Kasha, Characterization of electronic transitions in complex molecules, Discussions of the Faraday Society 9 (1950) 14-19.

[23] J.R. Lakowicz, Introduction to Fluorescence, Principles of Fluorescence Spectroscopy, Springer, USA, 2006, pp. 1-26.

[24] M. Milas, M. Rinaudo, M. Knipper, J.L. Schuppiser, Flow and viscoelastic properties of xanthan gum solutions, Macromolecules 23 (1990) 2506-2511.

[25] J.W. McAllister, P.W. Schmidt, K.D. Dorfman, T.P. Lodge, F.S. Bates, Thermodynamics of Aqueous Methylcellulose Solutions, Macromolecules 48 (2015) 7205-7215.

[26] F. Freitas, V.D. Alves, J. Pais, N. Costa, C. Oliveira, L. Mafra, L. Hilliou, R. Oliveira, M.A.M. Reis, Characterization of an extracellular polysaccharide produced by a Pseudomonas strain grown on glycerol, Bioresource Technology 100 (2009) 859-865.

[27] P. Larkin, Chapter 6 - IR and Raman Spectra-Structure Correlations: Characteristic Group Frequencies, Infrared and Raman Spectroscopy, Elsevier, Oxford, 2011, pp. 73-115.

[28] E. Wiercigroch, E. Szafraniec, K. Czamara, M.Z. Pacia, K. Majzner, K. Kochan, A. Kaczor, M. Baranska, K. Malek, Raman and infrared spectroscopy of carbohydrates: A review, Spectrochimica Acta Part A: Molecular and Biomolecular Spectroscopy 185 (2017) 317-335.

[29] J. Wang, P. Somasundaran, Study of galactomannose interaction with solids using AFM, IR and allied techniques, Journal of Colloid and Interface Science 309 (2007) 373-383.

[30] B.C. Smith, An IR Spectral Interpretation Potpourri: Carbohydrates and Alkynes, Spectroscopy 32 (2017) 18-24.

[31] P. Larkin, Chapter 8 - Illustrated IR and Raman Spectra Demonstrating Important Functional Groups, Infrared and Raman Spectroscopy, Elsevier, Oxford, 2011, pp. 135-176.

[32] C. Fan, J. Tang, X. Zhou, Role of ammonium chloride in preparing poly(urea-formaldehyde) microcapsules using one-step method, Journal of Applied Polymer Science 129 (2013) 2848-2856.

[33] Determining Benzene Ring Substitution Patterns from IR Spectra, Spectra Analysis, 2008.

[34] T. Moschakis, B.S. Murray, E. Dickinson, Particle Tracking Using Confocal Microscopy to Probe the Microrheology in a Phase-Separating Emulsion Containing Nonadsorbing Polysaccharide, Langmuir 22 (2006) 4710-4719.

[35] E. Dickinson, Hydrocolloids at interfaces and the influence on the properties of dispersed systems, Food Hydrocolloids 17 (2003) 25-39.

[36] Q. Wang, S.W. Cui, Understanding the Physical Properties of Food Polysaccharides, in: S.W. Cui (Ed.) Food Carbohydrates Chemistry, Physical Properties, and Applications, CRC Press, Taylor & Francis Group, US, 2005.

[37] C.L. Butler, L.H. Cretcher, THE COMPOSITION OF GUM ARABIC1,2, Journal of the American Chemical Society 51 (1929) 1519-1525.

[38] D. Renard, L. Lavenant-Gourgeon, M.-C. Ralet, C. Sanchez, Acacia senegal Gum: Continuum of Molecular Species Differing by Their Protein to Sugar Ratio, Molecular Weight, and Charges, Biomacromolecules 7 (2006) 2637-2649.

[39] B.R. Nair, D.J. Francis, Kinetics and mechanism of urea-formaldehyde reaction, Polymer 24 (1983) 626-630.

[40] S. Peker-Baslara, B. Övez, Ö. Balcioǧlu, Properties of gelatin-gum arabic coacervates composited with amino resins, Journal of Chemical Technology & Biotechnology 56 (1993) 175-184.

[41] K. Shibatani, K. Fujii, Reaction of poly(vinyl alcohol) with formaldehyde and polymer stereoregularity. Model compounds, Journal of Polymer Science Part A-1: Polymer Chemistry 8 (1970) 1647-1656.

[42] R.C. Wilson, W.F. Pfohl, Study of cross-linking reactions of melamine/formaldehyde resin with hydroxyl functional polyester by generalized 2-D infrared spectroscopy, Vibrational Spectroscopy 23 (2000) 13-22.

[43] N. Garti, D. Reichman, Hydrocolloids as Food Emulsifiers and Stabilizers, Food Structure 12 (1993) 411-426.

[44] D. Saha, S. Bhattacharya, Hydrocolloids as thickening and gelling agents in food: a critical review, Journal of food science and technology 47 (2010) 587-597.

[45] A. Syrbe, W.J. Bauer, H. Klostermeyer, Polymer Science Concepts in Dairy Systems—an Overview of Milk Protein and Food Hydrocolloid Interaction, International Dairy Journal 8 (1998) 179-193.

[46] E. Dickinson, Hydrocolloids acting as emulsifying agents – How do they do it?, Food Hydrocolloids 78 (2018) 2-14.

[47] A.F. Olea, J.K. Thomas, Rate constants for reactions in viscous media: correlation between the viscosity of the solvent and the rate constant of the diffusion-controlled reactions, Journal of the American Chemical Society 110 (1988) 4494-4502.

[48] M.H. Friedman, Free Diffusion, Principles and Models of Biological Transport, Springer-Verlab, New York, 2008, pp. 29-65.
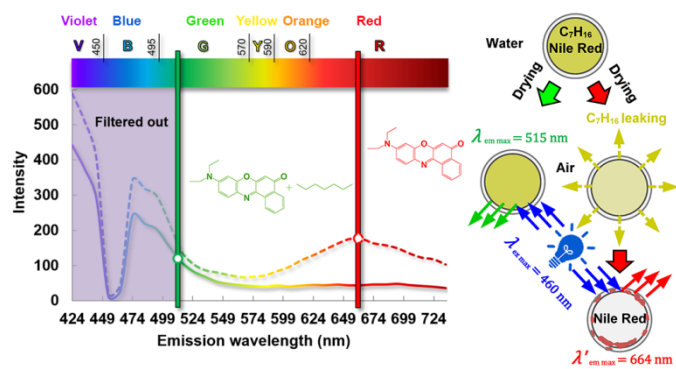
A fast fluorescent staining method is developed to confirm retention of volatile cargos

Free flowing spherical capsules with volatile phase change materials are formulated

Carboxyl or anhydride moieties on emulsifier molecules are not essential for encapsulation